

Möbius Strip Microlasers: A Testbed for Non-Euclidean Photonics

Yalei Song^{1,2}, Yann Monceaux¹, Stefan Bittner³, Kimhong Chao¹, Héctor M. Reynoso de la Cruz^{1,4}, Clément Lafargue¹, Dominique Decanini⁵, Barbara Dietz², Joseph Zyss¹, Alain Grigis⁶, Xavier Checoury⁵, and Melanie Lebental^{1,*}

¹Laboratoire Lumière, Matière et Interfaces (LuMIn) CNRS, ENS Paris-Saclay, Université Paris-Saclay, CentraleSupélec, 91190 Gif-sur-Yvette, France

²Lanzhou Center for Theoretical Physics and the Gansu Provincial Key Laboratory of Theoretical Physics, Lanzhou University, Lanzhou, 730000 Gansu, China

³Chair in Photonics, LMOPS EA-4423 Laboratory, CentraleSupélec and Université de Lorraine, 2 rue Edouard Belin, 57070 Metz, France

⁴Department of Physical Engineering, Academic Body of Statistical Mechanics, Science and Engineering Division of the University of Guanajuato, León, Gto. 36000, México

⁵Centre de Nanosciences et de Nanotechnologies, CNRS, Université Paris-Saclay, 10 Boulevard Thomas Gobert, 91120 Palaiseau, France

⁶Laboratoire d'Analyse, Géométrie et Applications, CNRS UMR 7539, Université Sorbonne Paris Cité, Université Paris 13, Institut Galilée, 99 avenue Jean-Baptiste Clément, 93430 Villetaneuse, France

 (Received 19 November 2020; accepted 10 September 2021; published 8 November 2021)

We report on experiments with Möbius strip microlasers, which were fabricated with high optical quality by direct laser writing. A Möbius strip, i.e., a band with a half twist, exhibits the fascinating property that it has a single nonorientable surface and a single boundary. We provide evidence that, in contrast to conventional ring or disk resonators, a Möbius strip cavity cannot sustain whispering gallery modes (WGM). Comparison between experiments and 3D finite difference time domain (FDTD) simulations reveals that the resonances are localized on periodic geodesics.

DOI: [10.1103/PhysRevLett.127.203901](https://doi.org/10.1103/PhysRevLett.127.203901)

The search for geodesic curves on manifolds of arbitrary dimension and metric has been a major driving force in mathematical physics from its inception at the beginning of the 20th century [1–3]. The classical work by J. L. Synge brought this domain in contact with general relativity [4]. In the 1970s, “trace formulas” were developed that provide a semiclassical approximation of the spectral density in terms of a sum over classical periodic trajectories, establishing a direct link between classical and quantum mechanics [5,6]. The seminal works of Balian [7] and Gutzwiller [8] were implemented in a broad diversity of physical systems, including electron transport [9], billiards [10], and nuclear physics [11]. For open wave systems, the modes are typically localized on certain classical trajectories [12]. Similarly, the motion of particles constrained to a compact Riemannian surface [13,14] of negative curvature is connected to classical geodesics via the Selberg trace formula [8,15].

Variational principles are of fundamental importance in physics and also at the origin of the trace formula. The stationary phase approximation relates the quantum (or wave) propagator to classical trajectories, which follow the principle of least action [5]. On curved surfaces, these trajectories are not straight lines but *geodesics*, which are the shortest paths between two points [16]. Surfaces of arbitrary local curvature provide a fascinating playground for

non-Euclidean optics. Only recently have advanced lithography technologies enabled the fabrication of three-dimensional (3D) surfaces with high optical quality and thicknesses down to 1 μm [17], confining light to propagation within a quasi-two-dimensional curved layer. Many open questions can be tackled regarding the structure of the electromagnetic field in non-Euclidean resonators [18–21], which are also of relevance in other wave-related research fields like acoustics [22], hydrodynamics, gravity, or quantum physics.

Some aspects of quantum-mechanical systems can be investigated with electromagnetic systems thanks to the equivalence of the Schrödinger and Helmholtz equations. Prominent examples include billiard systems and their experimental implementations with microwave resonators [6], dielectric resonators [23,24], and microlasers [25], with ramification extending from applied to mathematical physics [26–28]. Organic microlasers provide an ideal testbed for studying ray-wave correspondence: with a typical size in the range of 50–200 μm , much larger than the wavelength, they operate in the semiclassical regime.

In this Letter, we explore the emerging domain of non-Euclidean photonics with Möbius strip microlasers fabricated by direct laser writing, see Fig. 1. Möbius strips have captured the attention of generations of scientists, from pure mathematics to physical, chemical, and engineering

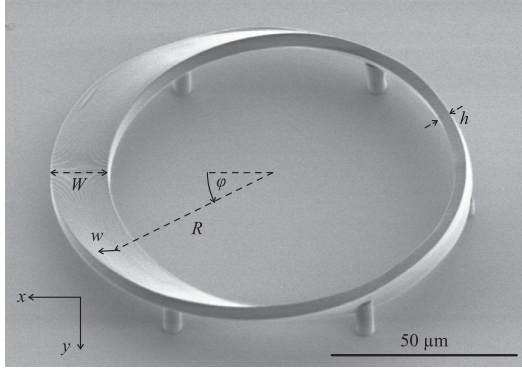


FIG. 1. SEM image of a Möbius strip microlaser with radius $R = 50 \mu\text{m}$, width $W = 15 \mu\text{m}$, and thickness $h = 3 \mu\text{m}$.

sciences [19,29–33]. A Möbius strip is formed by connecting two ends of a strip after twisting one end by 180° , whereas connecting them without twist results in a normal ring resonator. In spite of its simplicity, it exhibits peculiar topological properties because it has a single, nonorientable surface and a single boundary. In particular, a Möbius microcavity cannot display whispering gallery modes (WGMs). Normal ring resonators feature high- Q WGMs that propagate along the outer circular boundary. The trace formula relates WGMs to periodic ray orbits in the form of regular polygons with reflections at the outer boundary [23,34]. However, such classical trajectories do not exist in a Möbius strip because its boundary exhibits both concave

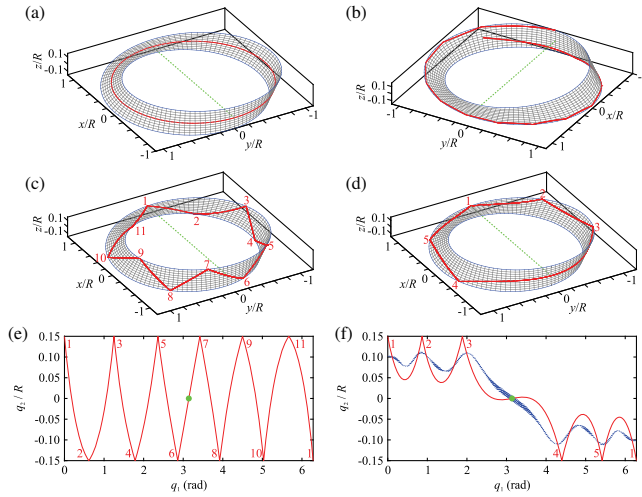


FIG. 2. Examples of trajectories on a Möbius strip with $W/R = 0.3$. The rotation symmetry axis $y = z = 0$ is indicated in green (dashed lines or dots). (a) Path along the center line of the Möbius strip. It is *not* a geodesic. (b) Trajectory along the boundary of the Möbius strip. It has to cross over to the “opposite” side at concave boundary parts. (c),(e) A periodic geodesic with 11 vertices and length $L = 7.031R$. (d),(f) Periodic geodesic 5a with five vertices and length $L = 6.732R$. The blue dotted line is the mean position calculated from Eq. (9) for the wave function in Fig. 6.

and convex parts, see Fig. 2(b). We provide evidences that, instead, its low-loss resonances are localized on periodic geodesics.

Möbius fabrication and parametrization.—The Möbius strip was designed by rotating a rectangle by 180° while its center travels along a circle of radius R . The geometric parameters are explained in Fig. 1. The width is fixed $W = 15 \mu\text{m}$. The radius R varies from 40 to 60 μm , and the thickness h varies from 1 to 5 μm .

The microlasers were fabricated by direct laser writing lithography using a Photonic Professional GT system with negative resist IP-G780 from the Nanoscribe company [17]. The resist was doped by 0.5 wt% pyromethene 597 laser dye (by the company Exciton), which is homogeneously distributed in the bulk host resist [35]. Each cavity is supported by six circular pylons to avoid coupling with the glass substrate. A scanning electron microscope (SEM) image of a Möbius strip microlaser is shown in Fig. 1.

A standard parametrization of a Möbius strip surface $\vec{r} = \vec{F}(\varphi, w)$ is

$$x = F_x(\varphi, w) = \left(R + w \cos \frac{\varphi}{2} \right) \cos \varphi, \quad (1)$$

$$y = F_y(\varphi, w) = \left(R + w \cos \frac{\varphi}{2} \right) \sin \varphi, \quad (2)$$

$$z = F_z(\varphi, w) = w \sin \frac{\varphi}{2}, \quad (3)$$

with $w \in [-W/2; W/2]$ and $\varphi \in [0; 2\pi]$, which yields a Möbius strip like in Fig. 1. A Möbius strip can be twisted the other way, which corresponds to adding a minus sign on line (2). We checked that the experiments and their interpretation are consistent for both chiralities.

Note that this parametrization differs from a Möbius strip constructed from a twisted paper sheet [36]. Since the latter can be unfolded to a flat plane, we call it a *flat* Möbius strip, see the Supplemental Material [37]. This has important consequences for geodesics and mode localization, which will be discussed below.

The Möbius strip microlasers were pumped individually and with uniform intensity by a beam perpendicular to the substrate from a frequency doubled Nd:YAG laser (532 nm, 500 ps, 10 Hz). Their emission was analyzed by a spectrometer coupled to a CCD camera with an overall resolution of 0.03 nm. The experiments were carried out at room pressure and temperature.

The inset of Fig. 3 shows a laser threshold at 5 MW/cm². This value decreases with increasing size of the Möbius strip, because of a larger gain volume collecting more pump light, and is similar to the laser threshold of 3D cavities made of the same laser dye with an equivalent gain volume [35].

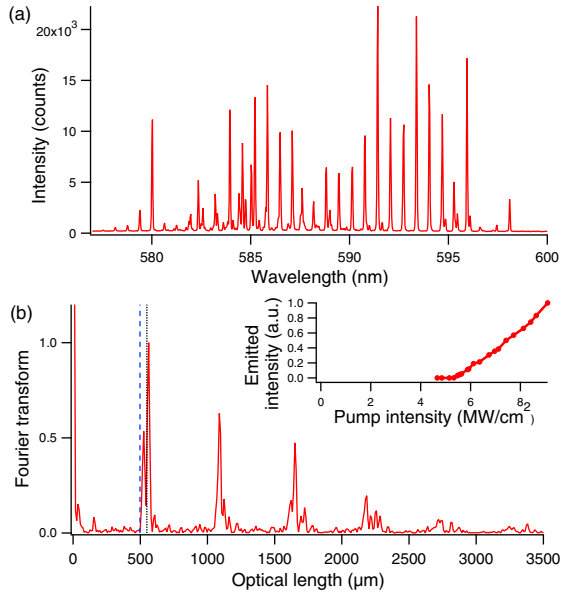


FIG. 3. (a) Experimental laser spectrum of a Möbius strip with $R = 50 \mu\text{m}$ and $h = 1 \mu\text{m}$ (1 s exposure). (b) Normalized Fourier transform (from wave number k to optical length) of the spectrum in (a). The vertical lines are at the optical lengths of half the perimeter (dashed blue line) and of the geodesic $5a$ (black dotted line) for $n_g = 1.58$. Inset: experimental threshold curve for a Möbius microcavity with $R = 50 \mu\text{m}$ and $h = 3 \mu\text{m}$.

The microlaser light is mostly emitted parallel to the substrate plane, and the emission mainly originates from the lateral boundaries of the strip at a near-grazing angle, see Fig. S9 in the Supplemental Material [37]. This is observed from all directions, which is consistent with modes confined inside the Möbius strip and propagating within this curved and twisted guiding layer.

A laser emission spectrum is shown in Fig. 3(a). It does not significantly depend on the direction of observation, but depends on the thickness h [37]. For $h = 1 \mu\text{m}$, it features a single series of equidistant resonances, which reveals information on the mode localization.

Helmholtz equation.—In Cartesian coordinates, the electric field fulfills the Helmholtz equation

$$(\Delta + n^2 k^2) \vec{E} = \vec{0}, \quad (4)$$

where k is the wave number in vacuum and n is the refractive index, which is 1 outside of the strip and $n \simeq 1.5$ inside it [38]. As the fabrication method does not generate stress in the resist, n is assumed to be homogeneous within the strip. Although it is experimentally evidenced that the laser emission of a Möbius microcavity is polarized, for the sake of simplicity, we will only consider a single electric field component ψ .

To map the Helmholtz equation (4) onto the Möbius surface, we introduce a local coordinate system (q_1, q_2, q_3) defined by the local frame $(\vec{u}_1, \vec{u}_2, \vec{u}_3)$ with

$$\vec{u}_1 = \frac{\partial \vec{F}}{\partial \varphi}, \quad \vec{u}_2 = \frac{\partial \vec{F}}{\partial w}, \quad \vec{u}_3 = \frac{\vec{u}_1 \times \vec{u}_2}{\|\vec{u}_1 \times \vec{u}_2\|}. \quad (5)$$

By construction, \vec{u}_1 and \vec{u}_2 lie within the strip, whereas \vec{u}_3 is orthogonal to it. For the Möbius strip considered here, $(\varphi, w) = (q_1, q_2)$.

We deal with the finite, but small thickness ($h = 1 \mu\text{m}$) of the Möbius strip by introducing an effective refractive index [39], assuming that the direction q_3 perpendicular to the strip can be separated from the directions (q_1, q_2) within the strip. Solving the equation in the q_3 direction yields the effective index for the phase velocity of a wave guided within the Möbius strip. We extend the effective index n_{eff} , originally introduced for flat layers, to a curved layer following Ref. [40]. The derivation is described in the Supplemental Material [37], where it is shown that the correction due to the curvature is negligible for the range of parameters considered in the experiments.

With these approximations, the wave equation reduces to a two-dimensional Helmholtz equation within the strip,

$$\Delta_s \psi_s + n_{\text{eff}}^2 k^2 \psi_s = 0, \quad (6)$$

where ψ_s depends only on (q_1, q_2) . The Laplace operator Δ_s in the curvilinear coordinate system is given by

$$\Delta_s \psi = \frac{1}{\sqrt{g}} \sum_{i,j=1}^2 \frac{\partial}{\partial q_i} \left(\sqrt{g} g^{ij} \frac{\partial \psi}{\partial q_j} \right), \quad (7)$$

with $g_{ij} = (\vec{u}_i \cdot \vec{u}_j)$ as the metric tensor, (g^{ij}) as its inverse, and $g = \det(g_{ij})$.

Based on this approximation [41], we consider the propagation of rays with an effective index n_{eff} in the curved surface defined by (\vec{u}_1, \vec{u}_2) . Since the radius R and the width W of the strip are large compared to the wavelength, a semiclassical approach is valid. The resonant modes should hence be related to periodic geodesics.

Geodesics.—A classical trajectory γ on a surface can be represented by a path $q(s) = [q_1(s), q_2(s)]$ with $s \in [0, 1]$; $q(0)$ is the initial point and $q(1)$ is the final point. This trajectory γ is a geodesic if its length is stationary with respect to variations of the path $q(s)$ while maintaining $q(0)$ and $q(1)$. The length is given by [16]

$$L_\gamma = \int_0^1 ds \left[\sum_{i,j} g_{ij}[q(s)] \frac{dq_i}{ds}(s) \frac{dq_j}{ds}(s) \right]^{1/2}, \quad (8)$$

with $i, j = 1, 2$. Since the geodesics on the Möbius strip cannot be derived analytically, we calculated them numerically using this variational principle [37].

A geodesic is periodic if $q(0) = q(1)$ and $dq/ds(0) = dq/ds(1)$. In contrast to the flat Möbius billiard [37], all periodic geodesics have at least one reflection on the boundary and are isolated [42]. Another striking difference

is the sequence of reflections on the boundary. In the flat Möbius billiard, the geodesics have consecutive reflections on opposite sides [43]; that is, a reflection with $q_2 = +W/2$ is always followed by one with $q_2 = -W/2$ and vice versa. Such periodic geodesics exist in the Möbius strip as well, but only if they have at least 11 reflections, see Fig. 2(c). As illustrated in Fig. 2(d), it also hosts periodic geodesics with consecutive reflections on the same side, a feature specific to the 3D Möbius strip. The geodesic of Fig. 2(d) is called “geodesic 5a” to distinguish it from other periodic geodesics with five reflections and similar length. Hereafter, we will compare it to experiments and numerical simulations.

Spectrum analysis.—The equidistant resonances in Fig. 3(a) indicate that the lasing modes are longitudinal modes located along a single classical trajectory or a few trajectories with similar lengths. To verify this conjecture, we analyze the spectra.

The distance Δk between two adjacent peaks is related to the geometric length L of this classical trajectory via $\Delta k = 2\pi/(n_g L)$ where n_g is the group refractive index [44]. Δk can be inferred from the Fourier transform, as illustrated in Fig. 3(b), which shows peaks at the optical length $n_g L$ and its harmonics. Hence we can determine the geometric length L if the group refractive index n_g is known. It is deduced from the effective index and contributions from the material dispersion of n and modal dispersion of n_{eff} . The three terms and their uncertainties are described in the Supplemental Material [37] and yield a group index of $n_g = 1.58 \pm 0.05$.

Figure 4 shows the measured optical lengths for twelve Möbius microlasers with radius $R = 50 \mu\text{m}$ and thickness $h = 1 \mu\text{m}$. Their clear disagreement with half the perimeter evidences that the lasing modes do not propagate along the cavity boundary as WGMs would do. In contrast, the agreement is very good for the geodesic 5a. A few other

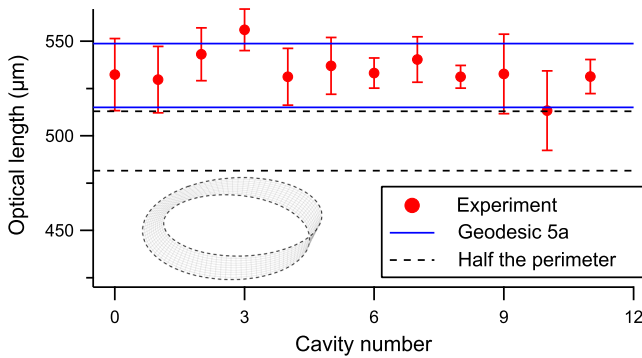


FIG. 4. Comparison of the experimental optical lengths for twelve Möbius microlasers with radius $R = 50 \mu\text{m}$ and thickness $h = 1 \mu\text{m}$ (red dots) with the optical length of geodesic 5a (continuous blue lines) and of the half perimeter (dashed black lines). The lower and upper lines correspond to the lower ($n_g = 1.53$) and upper ($n_g = 1.63$) limit of the group index n_g . Inset: the dashed line indicates the perimeter.

geodesics are also consistent with the experimental data. Some geodesics can be excluded because their length is too short or too long. This includes, for instance, all the geodesics with consecutive reflections on opposite sides, like the one in Fig. 2(c).

Wave functions.—Numerical simulations were performed with a homemade 3D finite difference time domain (FDTD) code for $R = 10 \mu\text{m}$, $W = 3 \mu\text{m}$, $h = 150 \text{nm}$, and $n = 1.515$. The aspect ratio W/R is the same as in the experiments. For these parameters, there is a single excitation in the vertical q_3 direction, but there exist several modes in the transverse w direction. The spectrum plotted in the inset of Fig. 5 features several branches of equidistant resonances. The Q factors of the low-loss modes (upper branch) are as high as 200 000. The spectrum is shown on a broader range in Fig. S5 of the Supplemental Material [37].

A typical wave function is plotted in Fig. 6. Because of the twofold rotational symmetry of the Möbius strip with respect to the x axis, the wave function must be odd or even with respect to rotation by 180° about it, i.e., about the green dot in Fig. 6(d). Consequently, the wave must cross from the upper side of the strip to the lower side, in contrast to a WGM, which would evolve along the boundary.

This wave function exhibits maximal intensity close to the boundary at positions coinciding with the reflections of the geodesic 5a, which is shown as a red line. To quantify the agreement, the mean position of the wave function along the strip width is calculated for each φ value,

$$\langle w \rangle(\varphi) = \frac{\iint_{\text{Half-plane}} w \rho(w, \varphi, q_3) dw dq_3}{\iint_{\text{Half-plane}} \rho(w, \varphi, q_3) dw dq_3}, \quad (9)$$

where $\rho = \frac{1}{2} \epsilon_0 \epsilon_r |\vec{E}|^2 + \frac{1}{2} \mu_0 |\vec{H}|^2$ is the energy density of the electromagnetic field. This mean position is plotted in Fig. 2(f). The agreement is very good, in particular, for the

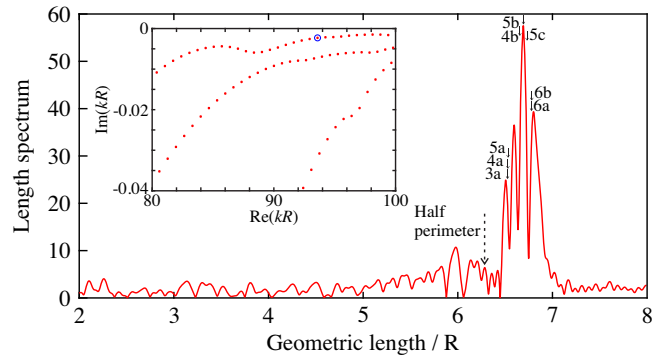


FIG. 5. Length spectrum derived from FDTD simulations for a Möbius strip with $R = 10 \mu\text{m}$, $W = 3 \mu\text{m}$, $h = 150 \text{nm}$, and $n = 1.515$. The dashed arrow indicates half the length of the perimeter. The solid arrows indicate the lengths of several periodic geodesics with 4 to 6 reflections. The inset shows part of the simulated spectrum, where the blue circle indicates the mode plotted in Fig. 6.

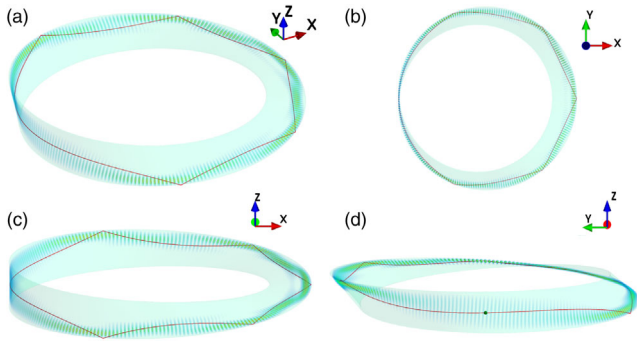


FIG. 6. (a)–(d) Different views of the same mode with $\text{Re}(kR) = 93.589$ and $\text{Im}(kR) = -0.0023$ ($Q = 20, 345$). $|\vec{E}|^2$ is shown in false colors. The geodesic 5a is superimposed as red lines. The green dot in (d) indicates the intersection of the x axis with the vertical section of the Möbius strip.

reflections on the boundary, further corroborating our claim that the modes are localized on periodic geodesics. More examples of wave functions are presented in the Supplemental Material [37].

The length spectrum in Fig. 5 is a Fourier transform of the simulated spectrum; see [37] for more information. It is peaked at the lengths of the periodic geodesics that were identified from the experiments and the wave functions, whereas there is no significant peak at the position of the half perimeter.

Conclusion.—Organic Möbius strip microlasers are investigated as nontrivial examples of non-Euclidean photonic structures fabricated by direct laser writing. We show that Möbius strip microlasers do not exhibit WGMs, in contrast to conventional ring cavities. Instead, their lasing modes are located on periodic geodesics. These findings are based on experiments, 3D FDTD numerical simulations, and on a dedicated algorithm to systematically identify the periodic geodesics. Our analysis is based on an effective index approximation that reduces the electromagnetic wave equation to a two-dimensional scalar Helmholtz equation. A future objective will be the derivation of a vectorial equation for the modes in curved surfaces and an in-depth investigation of the nontrivial polarization features [45] of such microlasers. This work opens the way to further explorations of non-Euclidean photonic devices.

This work was supported by the French RENATECH network, the CNano IdF DIM Nano-K, the Labex NanoSaclay (ANR-10-LABX-0035), and the Laboratoire International Associé ImagiNano. Y.S. and B.D. are supported by the National Natural Science Foundation of China under Grants No. 11775100, No. 11775101 and No. 11961131009. Furthermore, B.D. would like to thank ENS Paris-Saclay for financial support through MONABIPHOT Erasmus Mundus Master Course. Y.S. would like to thank the Laboratoire International Associé ImagiNano for financial support. S.B. acknowledges

support for the Chair in Photonics from Ministère de l'Enseignement Supérieur, de la Recherche et de l'Innovation, Région Grand-Est, Département Moselle, European Regional Development Fund (ERDF), Metz Métropole, GDI Simulation, CentraleSupélec, and Fondation CentraleSupélec. H. M. R. is supported by Consejo Nacional de Ciencia y Tecnología—México under Grant No. 2019-000016-01NACF-03530 of Movilidad Extranjera 2019, and the Dirección de Apoyo a la Investigación y el Posgrado (DAIP) Guanajuato under the Convocatoria de apoyo a posgrados-2019 Formato-B. J.-F. Audibert and H. K. Warner are acknowledged for the fabrication of centimeter-scale Möbius strips with a 3D printer, N. Pavloff for pointing out Ref. [13], P. Pansu, F. Jean, and G. Bossard for advices on geodesics, and E. Bogomolny for his derivation of the effective index approximation.

*lebental@ens-paris-saclay.fr

- [1] J. Hadamard, Les surfaces à courbures opposées et leurs lignes géodésiques, *J. Math. Pures Appl.* **4**, 27 (1898), <https://eudml.org/doc/235168>.
- [2] H. Poincaré, Sur les lignes géodésiques des surfaces convexes, *Trans. Am. Math. Soc.* **6**, 237 (1905).
- [3] T. Levi-Civita, Nozione di parallelismo in una varietà qualunque e conseguente specificazione geometrica della curvatura riemanniana, *Rend. Circ. Mat. Palermo* **42**, 173 (1916); *The Absolute Differential Calculus (Calculus of Tensors)* (Dover Publications, New York, 2013), Revised edition.
- [4] J.L. Synge, On the deviation of geodesics and null-geodesics, particularly in relation to the properties of spaces of constant curvature and indefinite line-element, *Ann. Math.* **35**, 705 (1934).
- [5] M. Brack and R.K. Bhaduri, *Semiclassical Physics* (Addison-Wesley Publishing Company, New York, 1997).
- [6] H.-J. Stöckmann, *Quantum Chaos, an Introduction* (Cambridge University Press, Cambridge, England, 1999).
- [7] R. Balian and C. Bloch, Distribution of eigenfrequencies for the wave equation in a finite domain: III. Eigenfrequency density oscillation, *Ann. Phys. (N.Y.)* **69**, 76 (1972).
- [8] M. C. Gutzwiller, *Chaos in Classical and Quantum Mechanics* (Springer, New York, 1990).
- [9] C. M. Marcus, A. J. Rimberg, R. M. Westervelt, P. F. Hopkins, and A. C. Gossard, Conductance Fluctuations and Chaotic Scattering in Ballistic Microstructures, *Phys. Rev. Lett.* **69**, 506 (1992).
- [10] M. V. Berry and M. Tabor, Calculating the bound spectrum by path summation in action-angle variables, *J. Phys. A* **10**, 371 (1977).
- [11] H. Olofsson, S. Åberg, O. Bohigas, and P. Leboeuf, Correlations in Nuclear Masses, *Phys. Rev. Lett.* **96**, 042502 (2006).
- [12] T. Harayama and S. Shinohara, Ray-wave correspondence in chaotic dielectric billiards, *Phys. Rev. E* **92**, 042916 (2015).

- [13] J. Goldstone and R. L. Jaffe, Bound states in twisting tubes, *Phys. Rev. B* **45**, 14100 (1992).
- [14] R. C. T. da Costa, Quantum mechanics of a constrained particle, *Phys. Rev. A* **23**, 1982 (1981).
- [15] R. Aurich, M. Sieber, and F. Steiner, Quantum Chaos of the Hadamard-Gutzwiller Model, *Phys. Rev. Lett.* **61**, 483 (1988).
- [16] W. Kühnel, *Differential Geometry. Curves—Surfaces—Manifolds*, 3rd ed. (American Mathematical Society, Providence, 2015).
- [17] J. Fischer and M. Wegener, Three-dimensional optical laser lithography beyond the diffraction limit, *Laser Photonics Rev.* **7**, 22 (2013).
- [18] V. H. Schultheiss, S. Batz, A. Szameit, F. Dreisow, S. Nolte, A. Tünnermann, S. Longhi, and U. Peschel, Optics in Curved Space, *Phys. Rev. Lett.* **105**, 143901 (2010).
- [19] J. Kreismann and M. Hentschel, The optical Möbius strip cavity: Tailoring geometric phases and far fields, *Europhys. Lett.* **121**, 24001 (2018).
- [20] A. Libster-Hershko, R. Shiloh, and A. Arie, Surface plasmon polaritons on curved surfaces, *Optica* **6**, 115 (2019).
- [21] C. Xu, I. Dana, L.-G. Wang, and P. Sebbah, Light chaotic dynamics in the transformation from curved to flat surfaces, [arXiv:2010.12220v2](https://arxiv.org/abs/2010.12220v2).
- [22] M. Avlund, C. Ellegaard, M. Oxborrow, T. Guhr, and N. Sondergaard, Observation of Periodic Orbits on Curved Two-Dimensional Geometries, *Phys. Rev. Lett.* **104**, 164101 (2010).
- [23] S. Bittner, E. Bogomolny, B. Dietz, M. Miski-Oglu, P. Oria Iriarte, A. Richter, and F. Schäfer, Experimental test of a trace formula for two-dimensional dielectric resonators, *Phys. Rev. E* **81**, 066215 (2010); S. Bittner, E. Bogomolny, B. Dietz, M. Miski-Oglu, and A. Richter, Application of a trace formula to the spectra of flat three-dimensional dielectric resonators, *Phys. Rev. E* **85**, 026203 (2012).
- [24] H. Cao and J. Wiersig, Dielectric microcavities: Model systems for wave chaos and non-Hermitian physics, *Rev. Mod. Phys.* **87**, 61 (2015).
- [25] M. Leubental, N. Djellali, C. Arnaud, J.-S. Laurent, J. Zyss, R. Dubertrand, C. Schmit, and E. Bogomolny, Inferring periodic orbits from spectra of simply shaped microlasers, *Phys. Rev. A* **76**, 023830 (2007); E. Bogomolny, N. Djellali, R. Dubertrand, I. Gozhyk, M. Leubental, C. Schmit, C. Ulysse, and J. Zyss, Trace formula for dielectric cavities II: Regular, pseudo-integrable, and chaotic examples, *Phys. Rev. E* **83**, 036208 (2011).
- [26] B. Dietz, T. Klaus, M. Miski-Oglu, A. Richter, M. Bischoff, L. von Smekal, and J. Wambach, Fullerene C60 Simulated with a Superconducting Microwave Resonator and Test of the Atiyah-Singer Index Theorem, *Phys. Rev. Lett.* **115**, 026801 (2015).
- [27] M. Bellec, U. Kuhl, G. Montambaux, and F. Mortessagne, Topological Transition of Dirac Points in a Microwave Experiment, *Phys. Rev. Lett.* **110**, 033902 (2013).
- [28] M. C. Rechtsman, Y. Plotnik, J. M. Zeuner, D. Song, Z. Chen, A. Szameit, and M. Segev, Topological Creation and Destruction of Edge States in Photonic Graphene, *Phys. Rev. Lett.* **111**, 103901 (2013).
- [29] S. Tanda, T. Tsuneta, Y. Okajima, K. Inagaki, K. Yamaya, and N. Hatakenaka, A Möbius strip of single crystals, *Nature (London)* **417**, 397 (2002).
- [30] L.-T. Huang and D.-H. Lee, Topological insulators on a Möbius strip, *Phys. Rev. B* **84**, 193106 (2011).
- [31] Z. Li and L. R. Ram-Mohan, Quantum mechanics on a Möbius ring: Energy levels, symmetry, optical transitions, and level splitting in a magnetic field, *Phys. Rev. B* **85**, 195438 (2012).
- [32] Y. Yin, S. Li, V. Engemaier, E. S. Ghareh Naz, S. Giudicatti, L. Ma, and O. G. Schmidt, Topology induced anomalous plasmon modes in metallic Möbius nanorings, *Laser Photonics Rev.* **11**, 1600219 (2017).
- [33] Y. Zeng, Z.-Y. Wang, Y. Wu, L.-S. Lu, Y.-X. Wang, S.-J. Shi, and Q. Qiu, Plasmonic microcavity formed by the Möbius strip, *Chin. Phys. B* **26**, 037303 (2017).
- [34] S. M. Reimann, M. Brack, A. G. Magner, J. Blaschke, and M. V. N. Murthy, Circular quantum billiard with a singular magnetic flux line, *Phys. Rev. A* **53**, 39 (1996).
- [35] M. A. Guidry, Y. Song, C. Lafargue, R. Sobczyk, D. Decanini, S. Bittner, B. Dietz, L. Huang, J. Zyss, A. Grigis, and M. Leubental, Three-dimensional micro-billiard lasers: The square pyramid, *Europhys. Lett.* **126**, 64004 (2019).
- [36] J. Gravesen and M. Willatzen, Eigenstates of Möbius nanostructures including curvature effects, *Phys. Rev. A* **72**, 032108 (2005).
- [37] The Supplemental Material at <http://link.aps.org/supplemental/10.1103/PhysRevLett.127.203901>, describes periodic orbits of the flat Möbius billiard as well as the algorithm that was implemented to find periodic geodesics for the 3D Möbius strip. This algorithm can be used for any smooth surface. Periodic geodesics of the 3D Möbius strip are further discussed in comparison with those of the flat Möbius billiard. Details on the 3D FDTD simulations are provided and additional wave functions are shown. The derivation of the effective index approximation for curved layers is described and experimental spectra for different thicknesses are compared.
- [38] T. Gissibl, S. Wagner, J. Sykora, M. Schmid, and H. Giessen, Refractive index measurements of photoresists for three-dimensional direct laser writing, *Opt. Mater. Express* **7**, 2293 (2017).
- [39] Another approach would be to add a q_3 component to the parametrization equations (1)–(3), then to change from the Cartesian coordinate to the local coordinate system, and finally to shrink the thickness to zero or to a small h value. In [14], this method was employed for matter waves. For electromagnetic waves, the effective index approximation has been widely and successfully used for systems composed of flat dielectric layers.
- [40] R. S. Elliott, Azimuthal surface waves on circular cylinders, *J. Appl. Phys.* **26**, 368 (1955).
- [41] The surface parametrization (1)–(3) does not depend on q_3 . It follows that $g_{33} = 1$ and $g_{13} = g_{31} = g_{23} = g_{32} = 0$, and that the 3D curvilinear Laplace operator can be separated in two parts, namely, the propagation within the curved surface and the propagation orthogonal to the strip. In practice, the actual Möbius cavity has a nonvanishing thickness h , and both directions of propagation are coupled. It is assumed

that this coupling is negligible for a small thickness, thus allowing us to introduce the effective refractive index n_{eff} .

- [42] A periodic geodesic is called isolated if there is no other periodic geodesic in its vicinity.
- [43] The notion of same or opposite side makes sense from a local perspective only, since a Möbius strip actually has only one side.
- [44] N. Sobeshchuk, M. A. Guidry, C. Lafargue, R. Gashemi, D. Decanini, J. Zyss, and M. Lebental, Out-of-plane modes in three-dimensional Fabry-Perot microlasers, *Appl. Phys. Lett.* **112**, 261102 (2018).
- [45] T. Bauer, P. Banzer, E. Karimi, S. Orlov, A. Rubano, L. Marrucci, E. Santamato, R. W. Boyd, and G. Leuchs, Observation of optical polarization Möbius strips, *Science* **347**, 964 (2015).